Petroleum Science 20 (2023) 3478–3487

Contents lists available at ScienceDirect

Petroleum Science

journal homepage: www.keaipublishing.com/en/journals/petroleum-science

Original Paper

Effects of CH_4/CO_2 multi-component gas on components and properties of tight oil during CO_2 utilization and storage: Physical experiment and composition numerical simulation

Zhi-Hao Jia [a], Ren-Yi Cao [a, *], Bin-Yu Wang [a], Lin-Song Cheng [a], Jin-Chong Zhou [a], Bao-Biao Pu [a], Fu-Guo Yin [a], Ming Ma [b]

[a] College of Petroleum Engineering, China University of Petroleum, Beijing, 102245, China
[b] The Pennsylvania State University, University Park, PA, 16802, USA

ARTICLE INFO

Article history:
Received 30 November 2022
Received in revised form
28 May 2023
Accepted 5 June 2023
Available online 6 June 2023

Edited by Yan-Hua Sun

Keywords:
Multi-component gas
Properties and components
Core displacement experiment
Nano-confinement numerical simulation
CO_2 utilization and storage

ABSTRACT

An essential technology of carbon capture, utilization and storage-enhanced oil recovery (CCUS-EOR) for tight oil reservoirs is CO_2 huff-puff followed by associated produced gas reinjection. In this paper, the effects of multi-component gas on the properties and components of tight oil are studied. First, the core displacement experiments using the CH_4/CO_2 multi-component gas are conducted to determine the oil displacement efficiency under different CO_2 and CH_4 ratios. Then, a viscometer and a liquid density balance are used to investigate the change characteristics of oil viscosity and density after multi-component gas displacement with different CO_2 and CH_4 ratios. In addition, a laboratory scale numerical model is established to validate the experimental results. Finally, a composition model of multi-stage fractured horizontal well in tight oil reservoir considering nano-confinement effects is established to investigate the effects of multi-component gas on the components of produced dead oil and formation crude oil. The experimental results show that the oil displacement efficiency of multi-component gas displacement is greater than that of single-component gas displacement. The CH_4 decreases the viscosity and density of light oil, while CO_2 decreases the viscosity but increases the density. And the numerical simulation results show that CO_2 extracts more heavy components from the liquid phase into the vapor phase, while CH_4 extracts more light components from the liquid phase into the vapor phase during cyclic gas injection. The multi-component gas can extract both the light components and the heavy components from oil, and the balanced production of each component can be achieved by using multi-component gas huff-puff.

1. Introduction

The recovery by traditional waterflooding development for tight oil reservoir is inadequate because of nano pore-throat and extremely low permeability (Jia et al., 2012a, 2012b; Kuang et al., 2012; Yao et al., 2013; Zou et al., 2015; Zhou et al., 2019; Wang et al., 2021). Gas injection development method is one of the key strategies for EOR of tight oil reservoir. Currently, as a key carbon capture, utilization and storage-enhanced oil recovery (CCUS-EOR) technique, cyclic CO_2 injection can not only achieve effective development of tight oil, but also achieve CO_2 utilization and storage (Harpalani and Mitra, 2010; Riazi et al., 2011; Pang et al., 2012; Han et al., 2016; Wang et al., 2017a). The simulation results of cyclic CO_2 injection in tight reservoirs show that the recovery efficiency can be increased by more than 20% (Pu et al., 2016; Yu et al., 2016, 2017; Song and Yang, 2017). However, the utilization and storage efficiency of CO_2 are significantly decreased after multiple rounds of cyclic CO_2 injection. As a result, numerous scholars proposed CO_2 injection followed by associated produced gas reinjection. The main components of associated produced gas are CH_4 and CO_2. This method could considerably enhance both the oil recovery and the effective CO_2 storage volume (Al Hinai et al., 2019; Yu et al., 2020; Zhang et al., 2020; Jokar et al., 2021; Li et al., 2021).

* Corresponding author.
E-mail address: caorenyi@126.com (R.-Y. Cao).

https://doi.org/10.1016/j.petsci.2023.06.002

The single-component gas used in the process of gas injection generally includes CO_2, CH_4, N_2, etc. (Alquriaishi and Shokir, 2011; Zhang et al., 2018a; Yu et al., 2019; Qiu et al., 2020; Wei et al., 2020; Zhu et al., 2021). After CO_2 dissolving in formation oil, its viscosity will decrease to one tenth of its original value, and the increase in formation pressure caused by CO_2 injection will further improve the solubility of CO_2 and further reduce the viscosity of crude oil (Crawford et al., 1978). In addition, dissolved CO_2 can increase the volume of crude oil by 10–100 times (Guo et al., 2018). Generally, CO_2 is in a supercritical phase state under the initial temperature and pressure conditions of oil reservoir. The hydrocarbon components of crude oil can be extracted to realize miscibility (Al-Riyami et al., 2017). The EOR mechanism of CH_4 is similar to that of CO_2. The viscosity of crude oil can also be lowered by CH_4 dissolving (Liu et al., 1998). It can both extract light and medium components from crude oil, but its extraction efficiency is less than that of CO_2 (Luo et al., 2001). CH_4 has better compatibility with reservoir crude oil and can perform relatively favorable component mass transfer (Lakatos et al., 1999). However, the solubility of CH_4 in crude oil is relatively low, so it has certain advantages over CO_2 in maintaining formation pressure (Duiveman et al., 2005). N_2, unlike CO_2 and hydrocarbon gases, is primarily used to maintain formation pressure because it is neither soluble in water nor crude oil (Hudgins et al., 1990; Dindoruk et al., 1997; Janssen et al., 2018). The research mentioned above indicates that CO_2 has the best solubility and extraction effect, N_2 has the largest effect on preserving formation energy, and CH_4 is more compatible with reservoirs.

Due to the different EOR mechanisms of single-component gas, the multi-component gas injection technology could combine the advantages of different gases. Rich gas, flue gas, acid gas, and air, etc. are typical multi-component gas (Tuta and Singhal, 1998; Christensen et al., 2001; Rogers and Grigg, 2001; Dong and Huang., 2002; Wang et al., 2017b). Ning et al. (2011) studied the effects of CO_2 mixture with different propane fractions on heavy oil reservoir, and showed that propane can effectively increase the solubility of CO_2 to further decrease the oil viscosity. Shyeh-Yung and Stadler (1995) proposed that the propane will increase the solubility of N_2 and improve the oil displacement efficiency. Based on PVT analysis, Huang et al. (2019) investigated the compatibility of several gases (CO_2, associated gas, flue gas, and deoxygenated air) after water flooding and showed that the flue gas and the deoxygenated air are more suited for single well huff-puff. Through the analysis and discussion of gas injection method in shale reservoirs in the United States, Bender and Akin (2017) showed that flue gas injection followed by CO_2 injection can improve the economic benefits. Jia and Sheng (2017) showed that rapid air injection can produce the thermal effect more effectively and oxygen in the air will speed up the reaction of crude oil. According to the above research, the development performance of multi-component gas in tight oil reservoir is better than that of single-component gas.

The pore-throat of tight oil reservoirs is in nanoscale. Through theoretical research and a few experimental studies, many scholars have found that complex phase behavior will occur in the reservoir within the pore-throat radius of 1–50 nm (Ambrose et al., 2010; Assef et al., 2019; Teklu et al., 2014; Ally et al., 2016; Dong et al., 2016; Li and Firoozabadi, 2009; Pinho et al., 2014; Parsa et al., 2015). Among these, the analytic equation of state (EOS) method is currently a more complete phase prediction technique and can more effectively be used in numerical simulation. Through the use of the GCMC approach, Vishnyakov et al. (2001) related the pore-throat radius and Lennard Jones parameters to critical temperature and pressure. Yang and his coworker (Yang et al., 2019; Yang and Li, 2020) also proposed to quantitatively characterize the key parameter offsets in the nanopore fitted from experimental data. In order to get more precise prediction results, Zhang et al. (2018b) introduced the capillary force in the nanopores into the iterative computation of EOS. Singh et al. (2009) studied the change of gas–liquid critical properties in slit pores of inorganic substances such as graphite and mica by GCMC method, and linked this method with the pore-throat radius. Based on the above analysis, the majority of scholars believe that nanopores in tight reservoirs have an impact on the phase state of the fluid, mainly affecting the critical parameters (Song et al., 2020; Teklu et al., 2014; Tian et al., 2019; Zheng et al., 2021).

However, there are few studies of the change characteristics of components and physical properties of tight oil caused by the CH_4/CO_2 multi-component gas. In this paper, the multi-component gas displacement experiments and composition numerical simulation considering nano-confinement effects are used to determine the effects of CH_4/CO_2 multi-component gas on components and properties of tight oil.

2. Multi-component gas displacement experiment

2.1. Experimental materials and procedures

The oil sample used in experiments is from a tight oil reservoir in the Ordos Basin, China. The components of the oil sample are shown in Appendix A. The viscosity and the density are 2.24 mPa·s and 0.803 g/cm^3 (53.5 °C, 10 MPa), respectively. The light fraction C_1–C_3 and heavy fraction C_{11+} are about 47% and 32%, which indicate the oil sample is light oil. The experimental water is reconfigured by distilled water according to the ionic composition of formation water, which is also shown in Appendix A. Its density is 0.998 g/cm^3 and its total salinity is 49,779 mg/L. In this experiment, artificial tight cores are used. Five multi-component gas experiments with different CH_4 and CO_2 proportions are designed, which are shown in Table 1.

2.2. Experimental equipment and process

The experiments have been separated into two parts: the first part is the multi-component gas displacement experiments, and the second part is the oil density and viscosity test after multi-component gas displacement experiments. In the first part of experiments, the central device is the self-developed core displacement system, which consists of a core holder (Tuochuang Co., Ltd., 0–60 MPa) and a Thermostat (Tuochuang Co., Ltd., HWX-III, 0–180 °C). The driving system and the data collection system are both connected to the central device as well. Among them, the driving system mainly consists of an ISCO pump (Teledyne ISCO, Lincoln, NE, USA), an air compressor (OTS-500), and 500-mL intermediate containers. The data collection system is mainly used to record the pressure, oil/gas rate and oil/gas production total. The connection of the experimental apparatus is shown in Fig. 1. The experimental steps are as follows.

(1) Basic preparations: The materials for the experiment, such as the oil sample, water sample, core, etc., are prepared in accordance with the experimental designs, and the central device is connected and its airtightness is verified.
(2) Multicomponent gas configuration: This step is the key to the success of the displacement experiment. Firstly, two 500-mL intermediate containers filled with water and one 500-mL empty intermediate container are prepared and put in the thermostat, which is set to 53.5 °C. Then, the pump is connected to the top of water-filled intermediate containers and continues to inject water until the pressure of intermediate containers is 12 MPa. In addition, the gas cylinder is connected to the pressurization system, which is connected to

Table 1
Multi-component gas displacement experiments.

Core sample	Components of experiment gas	Porosity, %	Permeability, mD	Length of core, cm	Cross-sectional area of core, cm^2
1	CO_2	9	0.1	5.5	4.91
2	70% CO_2 + 30% CH_4	9	0.1	5.5	4.91
3	50% CO_2 + 50% CH_4	9	0.1	5.5	4.91
4	30% CO_2 + 70% CH_4	9	0.1	5.5	4.91
5	CH_4	9	0.1	5.5	4.91

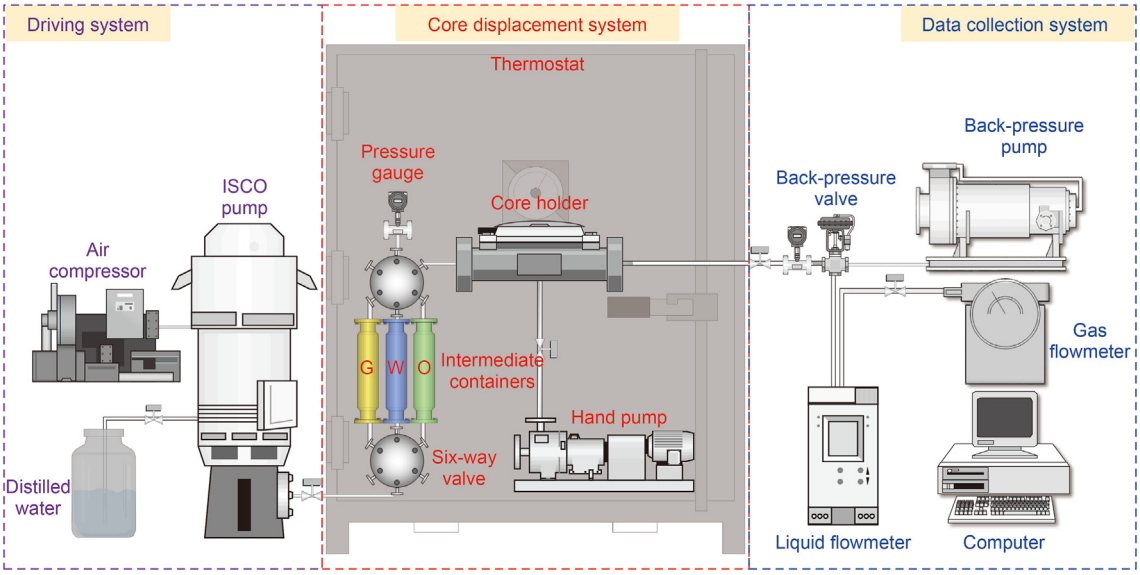

Fig. 1. Experimental apparatus for multi-component gas displacement, including a driving system, a core displacement system, and a data collection system.

the bottom of the water-filled intermediate container. The pressure of the pressurization system is set to 12 MPa. Next, all the valves are opened, and the water is squeezed out from the top of the intermediate container. The volume of each component gas is controlled by controlling the total volume of water being squeezed out. For example, if we want to configure a multi-component gas with a ratio of CH_4 to CO_2 of 3:7. The intermediate container connected to the CH_4 cylinder needs to extrude 150 mL of water, while the intermediate container connected to the CO_2 cylinder needs to extrude 350 mL of water. When the specific volume of the water is squeezed out, the valves connected to corresponding intermediate container should be immediately closed. Finally, the pump is used to fill the different gases from the two intermediate containers into the 500-mL empty intermediate container, and the top and bottom of which are linked to the central device and ISCO pump, respectively.

(3) Core vacuum saturation: The cores are placed into the chamber and vacuumed continuously for 10 h by a vacuum pump. Open the inlet valve to fill the saturation chamber with water. The process continues for a further 10 h to ensure that all of the gas has been pushed out of the core.

(4) Establishment of initial water saturation: The core is placed into the core holder and then saturated with formation oil by a constant-flux pump. The initial displacement rate is 0.1 mL/min, but it is increased to 0.5 mL/min when no water flowed out, until the oil production total reached 10 PV. Then, the cores are heated in the thermostat at 53.5 °C (formation temperature) for more than 4 h.

(5) Gas displacement and date analysis: The temperature is set to 53.5 °C, and the confining pressure is set to 10 MPa. Due to the difficulty in stably controlling the gas injection rate during the gas displacement, the constant pressure displacement method is used for the experiment. In addition, in order to eliminate the end-effect, the displacement pressure difference also needs to satisfy $\pi_1 \leq 0.6$. Finally, the displacement pressure difference is determined to be 11 MPa and the back pressure is set to be 1 MPa. The formula of π_1 is as follows:

$$\pi_1 = \frac{10^{-3}\sigma_{ow}}{\Delta P\sqrt{k_a/\phi}} \quad (1)$$

where σ_{ow} is the oil–water interfacial tension, mN/m; k_a is the absolute permeability, D; ϕ is the porosity; ΔP is the pressure difference, Pa.

The data collection system is adjusted and connected to the core displacement system. After the ISCO pump is turned on, the multi-component gas displacement experiments are started, and oil production total and gas production total are recorded at fixed intervals by liquid and gas flowmeter.

In the second part of the experiment, viscosimeter and density balance are used to measure the viscosity and density of crude oil before and after gas displacement, respectively, so as to determine the change characteristics of multi-component gas with different CH_4/CO_2 ratios on the physical properties of formation crude oil. The experimental steps are as follows.

(1) Viscosity test experiment: Under the temperature of 53.5 °C and the pressure of 10 MPa, the produced oil sample is directly transferred to the viscometer. The viscosity of crude oil is measured after full stirring and stabilization. The test

experiment is repeated three times, and the average value is used as the final value.

(2) Density test experiment: First, in order to balance the density balance, a clean glass cylinder is filled with the distilled cold water to 80% full, and is put in a 53.5 °C water bath. The glass hammer hanging on the scale end is immersed into the water in the glass cylinder and the density balance is adjusted to equilibrium. Then, under the temperature of 53.5 °C and the pressure of 10 MPa, the produced oil sample is directly transferred to the density balance. After emptying the water from the glass cylinder and wiping it clean, the test oil sample was loaded to the same height. The dry glass hammer was then sunk into the oil sample, and the vernier scale on the balance arm was adjusted to balance. This resulted in the relative density of the measured oil sample being obtained. Finally, the test experiment is repeated three times, and the average value is used as the test value.

2.3. Experimental result analysis

2.3.1. Characteristics of oil displacement efficiency

In all experiments, the oil displacement efficiency and gas–oil ratio (GOR) have similar characteristics in relation to injection volume. Fig. 2 shows the curve of oil displacement efficiency and GOR changing with injection volume in experimental program 1. With the increase in injection volume, the oil displacement efficiency increases dramatically followed by a period of stability, presenting a logarithmic curve trend. In stage I (0–0.2 PV), the GOR is stable at 30–40 m^3/m^3, and the oil displacement efficiency increases rapidly. The oil displacement efficiency in this stage accounts for about above 80% of the total oil displacement efficiency. In stage II (0.2–0.8 PV), the inflection points of oil displacement efficiency and GOR curve appeared, gas channeling appeared. This phenomenon shows that the oil displacement efficiency increased slowly, but the GOR increased rapidly. The oil displacement efficiency in this stage just accounts for about below 20% of the total oil displacement efficiency. In stage III (0.8–1.2 PV), the gas completely breaks through, and the GOR rapidly increases to 6000 m^3/m^3, and the oil displacement efficiency is almost unchanged.

A comparison of the oil displacement efficiency of different experiments shows that the ultimate oil displacement efficiency of tight reservoirs by gas displacement is above 50%. In addition, the displacement efficiency of multi-component gas is higher than that of single-component gas displacement. For multi-component gas displacement, with the increase in CH_4/CO_2 ratio, the oil displacement efficiency first increases and then decreases, presenting a quadratic polynomial curve trend, as shown in Fig. 3. When the ratio of CH_4 to CO_2 is about 50% (CH_4:CO_2 = 1:1), the oil displacement efficiency is maximum, which is above 60%.

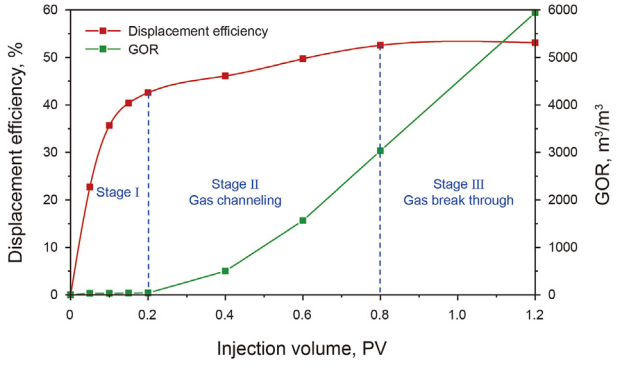

Fig. 2. Curves of oil displacement efficiency and GOR changing with injection volume in experimental program 1.

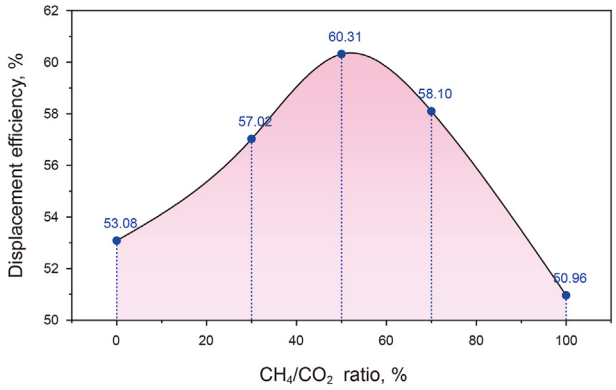

Fig. 3. The curve of oil displacement efficiency vs. CH_4/CO_2 ratio of multi-component gas.

2.3.2. Change characteristics of oil density and viscosity

Under the condition of initial formation temperature (53.5 °C) and pressure (10 MPa), the injected CO_2 and CH_4 are both in supercritical state. Therefore, injected gas significantly changes the density and viscosity of crude oil. The experimental results show that the supercritical CH_4 can decrease the viscosity and density of light oil, while the supercritical CO_2 will decrease the viscosity but increase the density of light oil. By comparing the results of different experiments, the viscosity and density of crude oil both decrease as the CH_4/CO_2 ratio of multi-component gas increases, as shown in Fig. 4. When the optimal CO_2/CH_4 ratio of 1:1 mentioned in the previous section is adopted, the oil viscosity decreases from 2.24 to 1.32 mPa·s, and the oil density decreases from 0.8030 to 0.7714 g/cm^3. Among them, the viscosity decreases by 41.03%, while the density only decreases by 3.94%.

3. Numerical simulation of multi-component gas displacement

3.1. PVTi fitting and phase state analysis considering nano-confinement effects

In order to further determine the effects of multi-component gas on components of crude oil during associated gas cycle-reinjection, the numerical simulation method has been used by the commercial compositional numerical simulator Eclipse300. The

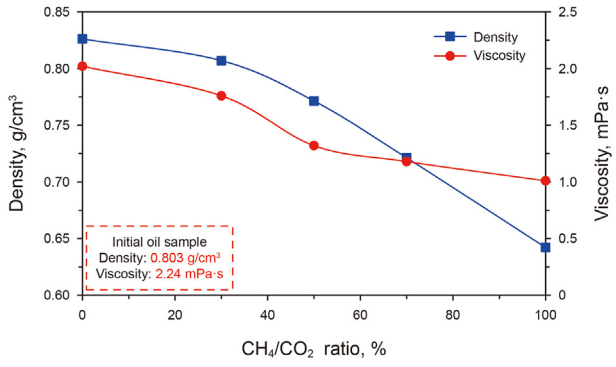

Fig. 4. Curves of density and viscosity vs. CH_4/CO_2 ratio of the multi-component gas.

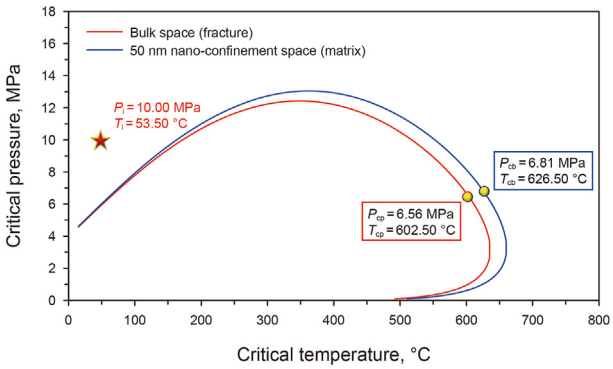

Fig. 5. Phase envelope of oil in matrix (50 nm nano-confinement space) and fracture (bulk space).

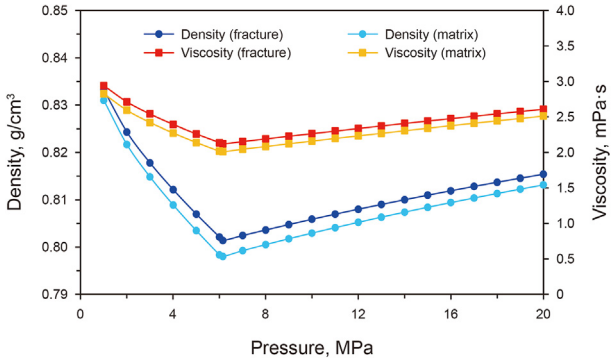

Fig. 6. Curves of density and viscosity of oil in matrix (50 nm nano-confinement space) and fracture (bulk space).

components are split by the Whitson method and reassembled into 11 pseudo-components. The Peng–Robinson equation of state (PR-EOS) and Lohrenz–Bray–Clark (LBC) model are used in numerical simulation. The thermodynamic properties of each component after PVTi fitting are shown in Appendix A. The pore-throat size of tight reservoirs ranges from several nanometers to hundreds of nanometers, which results in a significant difference between the phase state in the nano-confined space and that in the bulk space. Therefore, Singh's method (Singh et al., 2009) was used in this study to establish the correlation between the nano-pore size and the critical parameters inflection point. The expressions are as follows:

$$\Delta T_c^* = \frac{T_{cb} - T_{cp}}{T_{cb}} = 0.9409\frac{\delta_{lj}}{r_p} - 0.2415\left(\frac{\delta_{lj}}{r_p}\right)^2 \quad (2)$$

$$\Delta P_c^* = \frac{P_{cb} - P_{cp}}{P_{cb}} = 0.9409\frac{\delta_{lj}}{r_p} - 0.2415\left(\frac{\delta_{lj}}{r_p}\right)^2 \quad (3)$$

$$\delta_{lj} = 0.244\sqrt[3]{\frac{T_{cb}}{10P_{cb}}} \quad (4)$$

where ΔT_c^* is the relative critical temperature displacement, dimensionless; ΔP_c^* is the relative critical pressure displacement, dimensionless; r_p is the pore-throat radius, nm; T_{cb} is the critical temperature in bulk space, K; T_{cp} is the critical temperature in nano-confined space, K; P_{cb} is the critical pressure in bulk space, MPa; P_{cp} is the critical pressure in nano-confined space, MPa; δ_{lj} is Lennard–Jones size parameters, nm.

The mean radius of matrix pores is about 50 nm. As the critical pressure and critical temperature decreases in nano-confined space. The calculated phase envelope considering nano-confinement effects shrinks inward, as shown in Fig. 5.

Compared with bulk space, the viscosity and density of light oil in 50 nm nano-confined space both decrease. At the initial reservoir temperature and pressure, the oil density in nano-matrix decreases by about 0.36% and the oil viscosity in nano-matrix decreases by about 4.57%, as shown in Fig. 6.

3.2. Establishment of composition numerical model

The laboratory scale model and the model of multi-stage fractured horizontal well model have been established respectively by the commercial numerical simulator Eclipse300. The laboratory scale model is used to validate the used parameters of numerical simulation, such as thermodynamic parameters of each component, relative permeability curves, etc. And the parameters of laboratory scale model are totally the same as those of the cores in Section 2.1, which is shown in Fig. 7(a). The total size of the multi-stage fractured horizontal well model is 1600 m × 1000 m × 100 m. The numbers of grids in the *X*, *Y*, and *Z* directions are 251, 50, and 10, respectively. There is a 1400-m horizontal well with 20 fractures in the middle of model. The parameters of the multi-stage fractured horizontal well model are shown in Table 2. The nano-confinement effects in nano-matrix is considered and EOS partition is carried out

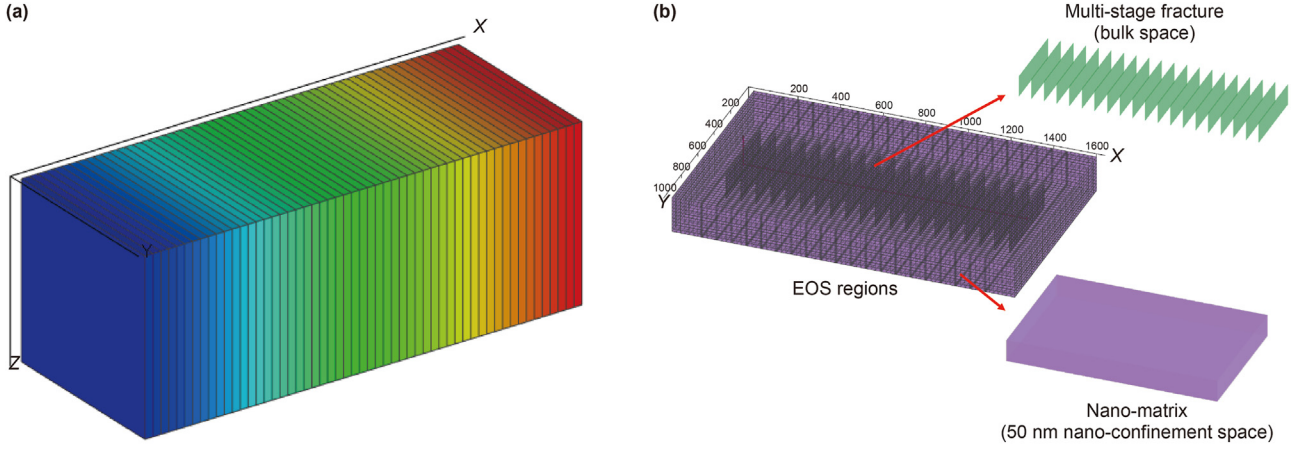

Fig. 7. 3D diagram of composition numerical simulation model. (**a**) Laboratory scale model; (**b**) Multi-stage fractured horizontal well model considering EOS partition.

Table 2
Parameters of the multi-stage fractured horizontal well model.

Parameter	Value	Parameter	Value
Top depth, m	1760	Initial pressure, MPa	10
Initial temperature, °C	53.5	Irreducible water saturation	0.24
Porosity of matrix, %	9	Porosity of fracture, %	2
Permeability of matrix, mD	0.1	Permeability of fracture, mD	1000
Fracture length, m	600	Fracture width, m	0.01
Injection BHP, MPa	12	Production BHP, MPa	1

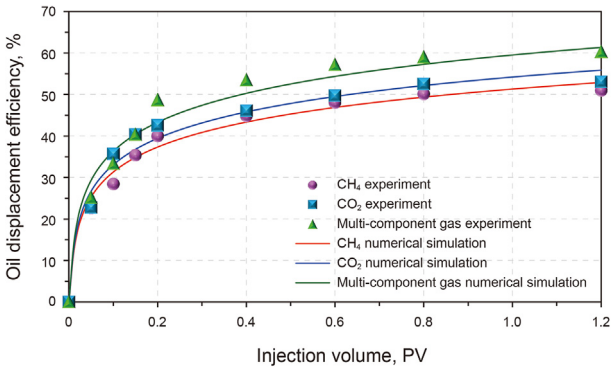

Fig. 8. Curves of oil displacement efficiency calculated by numerical simulation, which is validated by experimental results of gas displacement.

in the model, as shown in Fig. 7(b). This numerical simulation focuses on comparing the changes of components, density, and viscosity after pure component gas huff-puff (CH_4, CO_2) and multi-component gas huff-puff (50% CO_2 + 50% CH_4). The model is developed by 60 days of natural depletion followed by five rounds of gas huff-puff.

3.3. Laboratory scale model validation

In order to validate the reliability of the numerical simulation model and determine the parameters used in multi-stage fractured horizontal well model, the laboratory scale simulation has been carried out in this section. CH_4 displacement, CO_2 displacement, multi-component gas (50% CH_4 + 50% CO_2) displacement are simulated by laboratory scale models, respectively. We fit the numerical model with experimental results by modifying the rock and fluid parameters, which is shown in Fig. 8. Then, the modified rock and fluid parameters are used in the multi-stage fractured horizontal well model.

3.4. Result analysis and discussion

3.4.1. Distributions of oil components

The components, C_2, C_4–C_6 and C_{20+}, are selected as light hydrocarbon component, medium hydrocarbon component, and heavy hydrocarbon component. Fig. 9 shows the distributions of light, medium, heavy components in the liquid phase. Comparing the CO_2 huff-puff and CH_4 huff-puff, the sweep area of CO_2 huff-puff is smaller than that of CH_4 huff-puff. And CO_2 and CH_4 mainly spread in matrix near the fractures. However, CO_2 extracts more heavy components from oil, but CH_4 extracts more light components from oil during cyclic injection. This means heavy components are moved to the vapor phase with CO_2 injection, while light

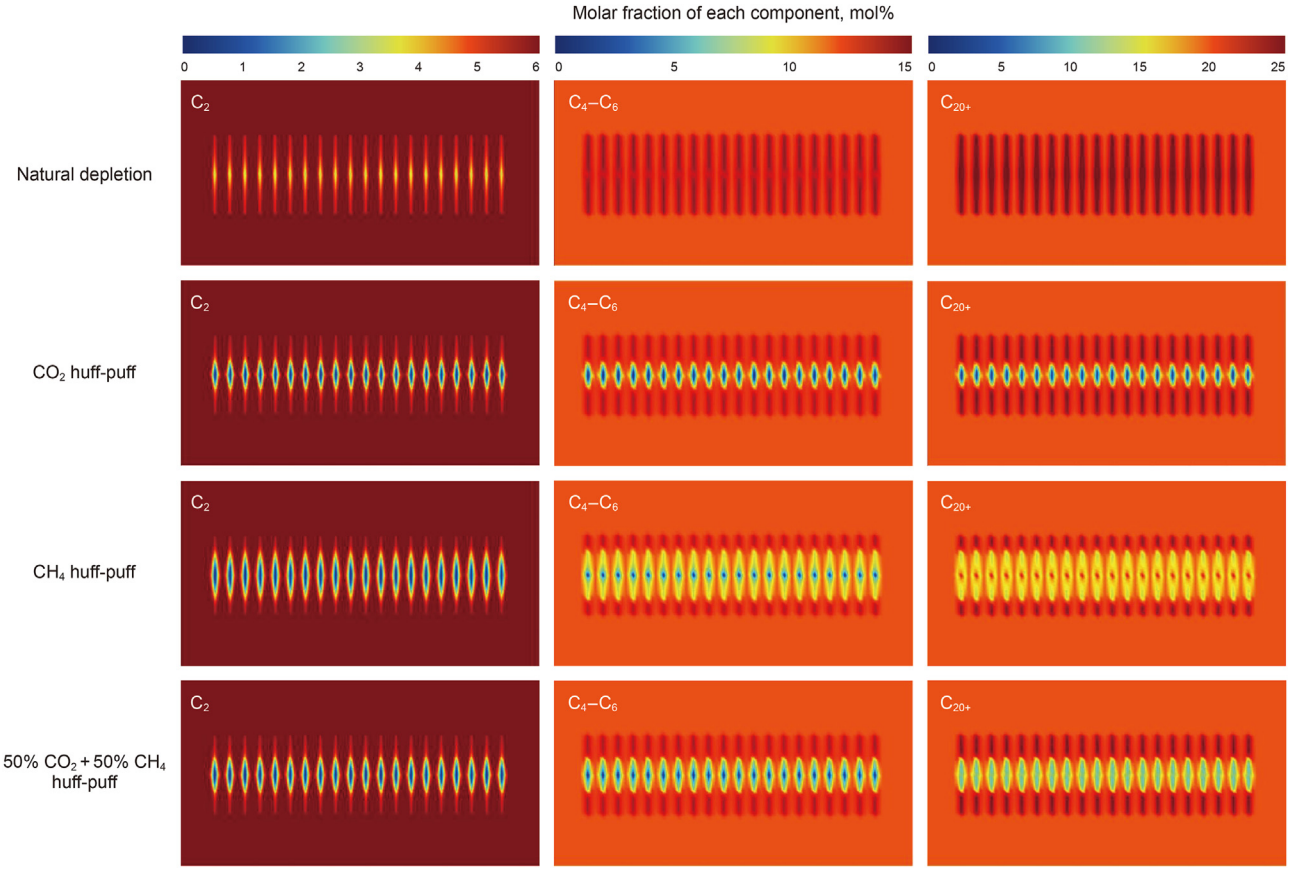

Fig. 9. Distributions of light, medium and heavy components in the liquid phase after different development methods.

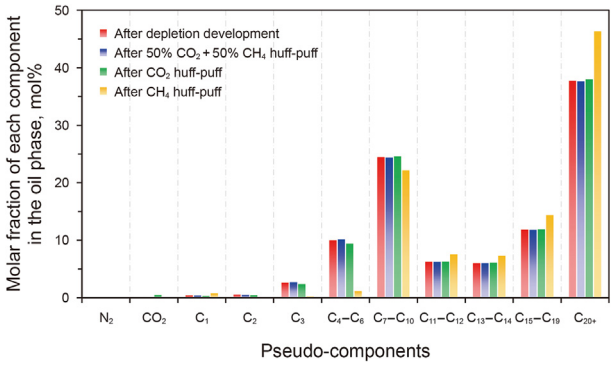

Fig. 10. Histogram of components of dead oil produced by different development methods, including natural depletion, CO_2 huff-puff, CH_4 huff-puff, and 50% CO_2 + 50% CH_4 huff-puff.

components are moved to the liquid phase with CH_4 injection. Therefore, multi-component gas could both extract the light components and heavy components from oil.

3.4.2. Component analysis of produced dead oil

Fig. 10 shows that the components of dead oil produced by different development methods at different stages. In the process of CH_4 huff-puff, gas production is higher and oil production is lower, indicating that CH_4 has a poor ability to replace crude oil. The components of dead oil produced by natural depletion are compared with those produced by 5 gas huff-puff cycles. After CH_4 huff-huff, the light components, C_2 and C_3, and the medium components, C_4–C_6, decrease rapidly, while the heavy components C_{11+} increase. The experimental result indicated the dead oil produced by CH_4 is getting heavier and heavier, and CH_4 could extract light and medium components from light oil. After CO_2 huff-huff, the light, medium components remained basically unchanged, while the C_{7+} components increase slightly, indicating that CO_2 could extract heavy components of crude oil. After 50% CO_2 + 50% CH_4 huff-puff, the components of produced dead oil have little change.

After multiple rounds of CH_4 huff-puff, the density and viscosity of the produced dead oil increases by 1.33% and 9.47%, respectively. After multiple rounds of CO_2 huff and puff, the density and viscosity of the produced dead oil increases by 0.08% and 1.00%, respectively, indicating that multiple rounds of CH_4 huff-puff and CO_2 huff-puff will lead to heavier component of produced dead oil. However, after multiple rounds of 50% CO_2 + 50% CH_4 huff-puff, the density and viscosity of the produced dead oil remain basically unchanged, thus effectively maintaining the high flow capacity of the produced dead oil, as shown in Fig. 11.

3.4.3. Component analysis of formation oil

The components of formation oil in fracture and matrix near the fracture under different development stages are compared, as shown in Fig. 12. In the process of natural depletion development, the molar fractions of light components, C_1, C_2, and C_3 in the oil phase decrease, while the medium and heavy components increase significantly, indicating that the light components are developed first and the heavy components remain in the formation. Furthermore, comparing the components of formation oil in the nano-matrix and the fracture, the molar fractions of light components in the oil phase in the matrix is greater than that in the fracture, while the molar fractions of light components in the oil phase in the matrix is less than that in the fracture, indicating that the light

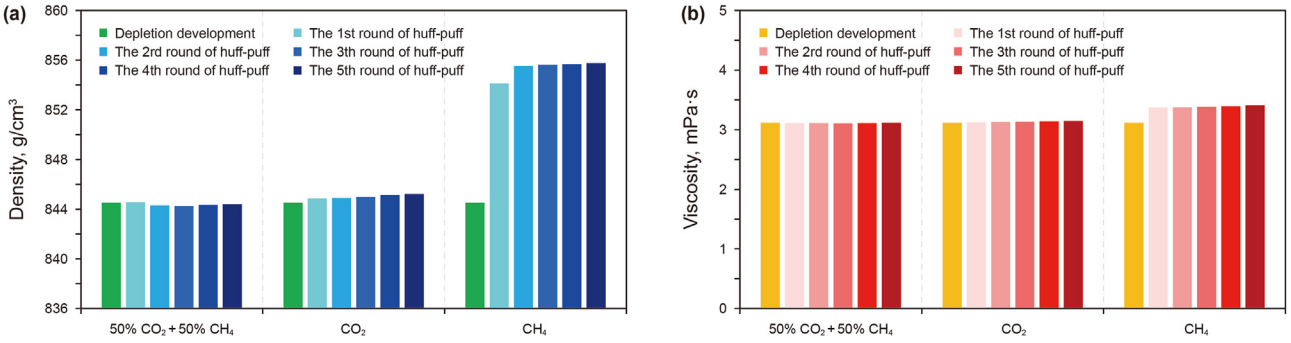

Fig. 11. Histograms of properties of dead oil produced by different development methods. (**a**) Density; (**b**) Viscosity.

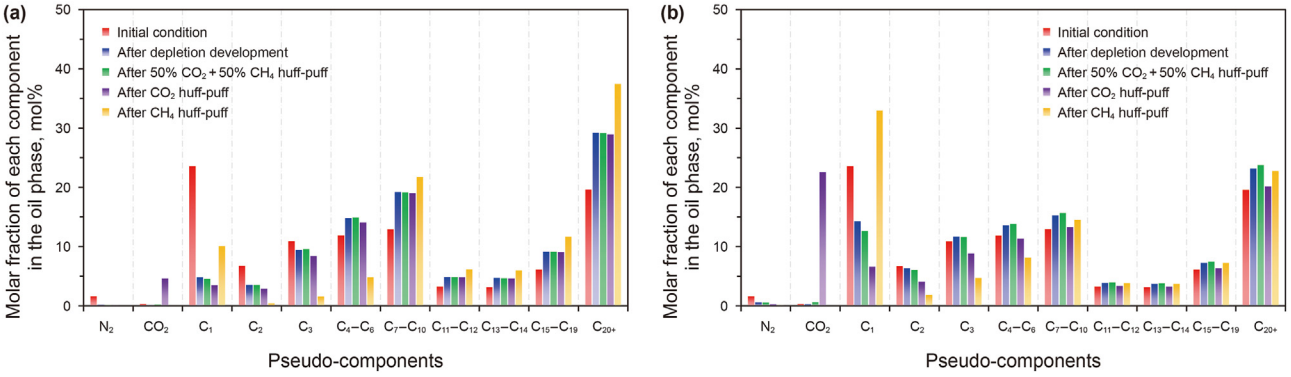

Fig. 12. Distribution histograms of components in formation oil phase under different development methods. (**a**) Formation oil in the fracture system (bulk space); (**b**) Formation oil in the matrix system (50 nm nano-confinement space).

components in the fracture are first produced and the light components in the matrix gradually flow into the fracture. By further comparing the component changes of formation oil after single-component gas huff-puff, it can be seen that CH_4 content in the matrix is greater than that in the fracture after CH_4 huff-puff, and CO_2 content in the matrix is also greater than that in the fracture after CO_2 huff-puff, indicating that the injected gas transfers to the matrix and extracts the hydrocarbon components of formation oil. Comparing the component changes of formation oil after depletion development and 50% CO_2 + 50% CH_4 huff-puff, it can be seen that the oil components in matrix and fracture remain basically unchanged, indicating that the balanced production of each component of crude oil can be achieved by using multi-component gas huff-puff.

4. Conclusions

In this paper, the effects of CH_4/CO_2 multi-component gas on the properties and components of crude oil are investigated through physical experiments and nano-confinement composition numerical simulation. The main conclusions of this work are as follows.

(1) The oil displacement efficiency of multi-component gas is higher than that of single-component gas. When the ratio of CH_4 to CO_2 is about 50% (CH_4: CO_2 = 1:1), the oil displacement efficiency is maximum.
(2) The supercritical CH_4 decreases the viscosity and density of light oil, while the supercritical CO_2 decreases the viscosity but increases the density of light oil. When the multi-component gas with 50% CO_2 and 50% CH_4 is used in displacement experiment, the oil viscosity decreases by 41.03%, while the oil density only decreases by 3.94%.
(3) CH_4 mainly extracts the light components from the liquid phase into the vapor phase, which leads to heavier component of produced dead oil and more gas production total. CO_2 mainly extracts the medium and heavy components from the liquid phase into the vapor phase, which leads to less heavy components in produced dead oil and more oil production total. CH_4/CO_2 multi-component gas can extract both the light components and heavy components from the liquid phase to the vapor phase, and the balanced production of each component can be achieved using multi-component gas huff-puff.

Declaration of competing interest

We declare that we have no financial and personal relationships with other people or organizations that can inappropriately influence our work, there is no professional or other personal interest of any nature or kind in any production, service and or company that could be construed as influencing the position presented in, or the manuscript entitled.

Acknowledgments

The authors acknowledge that this study was partially supported by the National Natural Science Foundation of China (No. 52174038 and No. 52004307), China Petroleum Science and Technology Project-major project-Research on tight oil-shale oil reservoir engineering methods and key technologies in Ordos Basin (ZLZX2020-02-04) and Science Foundation of China University of Petroleum, Beijing (No. 2462018YJRC015).

Appendix A. Composition of oil and water samples

The composition of oil and water samples used in experiments are shown in Table A1 and Table A2, respectively. The composition and thermodynamic properties used in composition numerical simulation are shown in Table A3.

Table A1
Composition of oil sample

Composition	Molar fraction of oil after flash separation, mol%	Molar fraction of gas after flash separation, mol%	Molar fraction of well fluid, mol%
N_2	0.000	3.262	1.615
CO_2	0.000	0.621	0.308
C_1	0.364	47.210	23.554
C_2	0.421	13.139	6.717
C_3	2.386	19.569	10.892
i-C_4	0.533	2.773	1.642
n-C_4	1.225	7.392	4.278
i-C_5	1.289	1.819	1.551
n-C_5	1.606	2.028	1.815
C_6	3.690	1.422	2.567
C_7	5.327	0.571	2.973
C_8	8.381	0.193	4.328
C_9	6.001	0.000	3.030
C_{10}	5.160	0.000	2.606
C_{11+}	63.617	0.000	32.125

Table A2
Ionic composition of formation water.

Composition, mg/L						Total salinity, mg/L
$K^+ + Na^+$	Ca^{2+}	Mg^{2+}	Cl^-	SO_4^{2-}	HCO_3^-	
16207	2528	270	29703	734	337	49779

Table A3
Thermodynamic properties of 11 pseudo-components after PVTi fitting

Pseudo-components	Molar fraction, mol%	Critical temperature, K	Critical pressure, MPa	Acentric factor	Molecular weight, g/mol	Critical volume, cm^3/g
N_2	1.615	126.200	3.394	0.040	28.013	88.750
CO_2	0.308	304.700	7.387	0.225	44.010	93.074
C_1	23.554	190.600	4.604	0.013	16.043	99.606
C_2	6.717	305.430	4.884	0.099	30.070	146.676
C_3	10.892	369.800	4.246	0.152	44.097	201.026
C_4–C_6	11.853	441.907	3.467	0.193	67.711	290.438
C_7–C_{10}	12.937	585.626	2.742	0.332	113.190	465.723
C_{11}–C_{12}	3.260	634.545	2.133	0.502	153.812	612.872
C_{13}–C_{14}	3.140	677.019	1.844	0.599	182.711	731.390
C_{15}–C_{19}	6.140	739.520	1.489	0.759	231.885	933.483
C_{20+}	19.584	1008.084	0.556	1.486	1092.880	4303.300

References

Al Hinai, N.M., Myers, M.B., Dehghani, A.M., Wood, C.D., Valdez, R., Jin, F., Xie, Q., Saeedi, A., 2019. Effects of oligomers dissolved in CO_2 or associated gas on IFT and miscibility pressure with a gas-light crude oil system. J. Petrol. Sci. Eng. 181, 106210. https://doi.org/10.1016/j.petrol.2019.106210.

Ally, J., Molla, S., Mostowfi, F., 2016. Condensation in nanoporous packed beds. Langmuir 32 (18), 4494–4499. https://doi.org/10.1021/acs.langmuir.6b01056.

Alquriaishi, A., Shokir, E., 2011. Experimental investigation of miscible CO_2 flooding. Petrol. Sci. Technol. 29 (19), 2005–2016. https://doi.org/10.1080/10916461003662976.

Al-Riyami, H.F., Kamali, F., Hussain, F., 2017. Effect of gravity on near-miscible CO_2 flooding. In: SPE Kingdom of Saudi Arabia Annual Technical Symposium and Exhibition doi:10.2118/188120-MS.

Ambrose, R.J., Hartman, R.C., Diaz-Campos, M., Akkutlu, I.Y., Sondergeld, C.H., 2010. New pore-scale considerations for shale gas in place calculations. In: SPE Unconventional Gas Conference. https://doi.org/10.2118/131772-MS.

Assef, Y., Kantzas, A., Almao, P.P., 2019. Numerical modelling of cyclic CO_2 injection in unconventional tight oil resources; trivial effects of heterogeneity and hysteresis in Bakken Formation. Fuel 236 (15), 1512–1528. https://doi.org/10.1016/j.fuel.2018.09.046.

Bender, S., Akin, S., 2017. Flue gas injection for EOR and sequestration: case study. J. Petrol. Sci. Eng. 157, 1033–1045. https://doi.org/10.1016/j.petrol.2017.07.044.

Christensen, J.R., Stenby, E.H., Skauge, A., 2001. Review of WAG field experience. SPE Reservoir Eval. Eng. 4 (2), 97–106. https://doi.org/10.2118/71203-PA.

Crawford, P.B., Reynolds, B., Rushing, M.D., Thomassom, B., 1978. Nitrogen may be used for miscible displacement in oil reservoirs. J. Petrol. Technol. 30 (12), 1715–1716. https://doi.org/10.2118/6445-PA.

Dindoruk, B., Orr, F.M., Johns, R.T., 1997. Theory of multicontact miscible displacement with nitrogen. SPE J. 2 (3), 268–279. https://doi.org/10.2118/30771-PA.

Dong, M., Huang, S., 2002. Flue gas injection for heavy oil recovery. J. Can. Petrol. Technol. 41 (9), 44–50. https://doi.org/10.2118/02-09-04.

Dong, X., Liu, H., Hou, J., Wu, K., Chen, Z., 2016. Phase equilibria of confined fluids in nanopores of tight and shale rocks considering the effect of capillary pressure and adsorption film. Ind. Eng. Chem. Res. 55 (3), 798–811. https://doi.org/10.1021/acs.iecr.5b04276.

Duiveman, M.W., Herwin, H., Grivot, P.G., 2005. Integrated management of water, lean gas, and air injection: the successful ingredients to EOR projects on the mature Handil Field. In: SPE Asia Pacific Oil and Gas Conference and Exhibition. https://doi.org/10.2118/93858-MS.

Guo, H., Dong, J., Wang, Z., Liu, H., Ma, R., Kong, D., Wang, F., Xin, X., Li, Y., She, H., 2018. EOR survey in China-Part 1. In: SPE Improved Oil Recovery Conference. https://doi.org/10.2118/190286-MS.

Han, J., Lee, M., Lee, W., Lee, Y., Sung, W., 2016. Effect of gravity segregation on CO_2 sequestration and oil production during CO_2 flooding. Appl. Energy 161, 85–91. https://doi.org/10.1016/j.apenergy.2015.10.021.

Harpalani, S., Mitra, A., 2010. Impact of CO_2 injection on flow behavior of coalbed methane reservoirs. Transport Porous Media 82, 141–156. https://doi.org/10.1007/s11242-009-9475-1.

Huang, K., Zhu, W., Sun, L., Wang, Q., Qing, L., 2019. Experimental study on gas EOR for heavy oil in Glutenite Reservoirs after water flooding. J. Petrol. Sci. Eng. 181, 106130. https://doi.org/10.1016/j.petrol.2019.05.081.

Hudgins, D.A., Llave, F.M., Chung, F.T.H., 1990. Nitrogen miscible displacement of light crude oil: a laboratory study. SPE Reservoir Eng. 5 (1), 100–106. https://doi.org/10.2118/17372-PA.

Janssen, M.T., Azimi, F., Zitha, P.L., 2018. Immiscible nitrogen flooding in Bentheimer Sandstones: comparing gas injection schemes for enhanced oil recovery. In: SPE Improved Oil Recovery Conference. https://doi.org/10.2118/190285-MS.

Jia, C., Zheng, M., Zhang, Y., 2012a. Unconventional hydrocarbon resources in China and the prospect of exploration and development. Petrol. Explor. Dev. 39 (2), 129–136. https://doi.org/10.1016/S1876-3804(12)60026-3.

Jia, C., Zou, C., Li, D., Zheng, M., 2012b. Assessment criteria, main types, basic features and resource prospects of the tight oil in China. Acta Pet. Sin. 33 (2), 343–350 (in Chinese). CNKI: SUN: SYXB.0.2012-03-000.

Jia, H., Sheng, J., 2017. Discussion of the feasibility of air injection for enhanced oil recovery in shale. Petroleum 3 (2), 249–257. https://doi.org/10.1016/J.PETLM.2016.12.003.

Jokar, S.M., Wood, D.A., Sinehbaghizadeh, S., Parvasi, P., Javanmardi, J., 2021. Transformation of associated natural gas into valuable products to avoid gas wastage in the form of flaring. J. Nat. Gas Sci. Eng. 94, 104078. https://doi.org/10.1016/j.jngse.2021.104078.

Kuang, L., Tang, Y., Lei, D., Chang, Q., Qu, Y., Hou, L., Liu, D., 2012. Formation conditions and exploration potential of tight oil in the Permian saline lacustrine dolomitic rock, Junggar Basin, NW China. Petrol. Explor. Dev. 39 (6), 700–711. https://doi.org/10.1016/S1876-3804(12)60095-0.

Lakatos, I., Bauer, K., Lakatos-Szabo, J., Puskas, S., Palasthy, G., Trömböczki, S., Kosztin, B., 1999. Injection of lean gases into light oil reservoirs: interfacial aspects. In: SPE Annual Technical Conference and Exhibition. https://doi.org/10.2118/56605-MS.

Li, D., Saraji, S., Jiao, Z., Zhang, Y., 2021. CO_2 injection strategies for enhanced oil recovery and geological sequestration in a tight reservoir: an experimental study. Fuel 284, 119013. https://doi.org/10.1016/j.fuel.2020.119013.

Li, Z., Firoozabadi, A., 2009. Interfacial tension of non-associating pure substances and binary mixtures by density functional theory combined with Peng–Robinson equation of state. J. Chem. Phys. 130 (15), 154108. https://doi.org/10.1063/1.3100237.

Liu, Z., Hou, J., Gao, Z., Wu, Y., 1998. The feasibility studies of natural gas flooding in Ansai Field. In: International Petroleum Conference and Exhibition. https://doi.org/10.2118/39885-MS.

Luo, K., Li, S., Zheng, X., Chen, G., Dai, Z., Liu, N., 2001. Experimental investigation into revaporization of retrograde condensate by lean gas injection. In: SPE Asia Pacific Oil and Gas Conference and Exhibition. https://doi.org/10.2118/68683-MS.

Ning, S., Jhaveri, B., Chambers, B., Jia, N., Gao, J., 2011. Viscosity reduction EOR with CO_2 & enriched CO_2 to improve recovery of Alaska North Slope viscous oils. In: SPE Western North American Region Meeting doi:10.2118/144358-MS.

Pang, J., Zuo, J., Zhang, D., Du, L., 2012. Impact of porous media on saturation pressures of gas and oil in tight reservoirs. In: SPE Canadian Unconventional Resources Conference. https://doi.org/10.2118/161143-MS.

Parsa, E., Yin, X., Ozkan, E., 2015. Direct observation of the impact of nanopore confinement on petroleum gas condensation. In: SPE Annual Technical Conference and Exhibition. https://doi.org/10.2118/175118-MS.

Pinho, B., Girardon, S., Bazer-Bachi, F., Bergeot, G., Marre, S., Aymonier, C., 2014. A microfluidic approach for investigating multicomponent system thermodynamics at high pressures and temperatures. Lab Chip 14 (19), 3843–3849. https://doi.org/10.1039/c4lc00505h.

Pu, W., Bing, W., Jin, F., Li, Y., Tang, Z., 2016. Experimental investigation of CO_2 huff-n-puff process for enhancing oil recovery in tight reservoirs. Chem. Eng. Res. Des. 111, 269–276. https://doi.org/10.1016/j.cherd.2016.05.012.

Qiu, Y., Wang, X., Liu, X., Cao, J., Liu, Y., Xi, B., Gao, W., 2020. In situ Raman spectroscopic quantification of CH_4–CO_2 mixture: application to fluid inclusions hosted in quartz veins from the Longmaxi Formation shales in Sichuan Basin, southwestern China. Petrol. Sci. 17, 23–35. https://doi.org/10.1007/s12182-019-00395-z.

Riazi, M., Sohrabi, M., Jamiolahmady, M., 2011. Experimental study of pore-scale mechanisms of carbonated water injection. Transport Porous Media 86, 73–86. https://doi.org/10.1007/s11242-010-9606-8.

Rogers, J., Grigg, R., 2001. A literature analysis of the WAG injectivity abnormalities in the CO_2 process. SPE Reservoir Eval. Eng. 4 (5), 375–386. https://doi.org/10.2118/73830-PA.

Shyeh-Yung, J., Stadler, M., 1995. Effect of injectant composition and pressure on displacement of oil by enriched hydrocarbon gases. SPE Reservoir Eng. 10 (2), 109–115. https://doi.org/10.2118/28624-PA.

Singh, S., Sinha, A., Deo, G., Singh, J., 2009. Vapor-liquid phase coexistence, critical properties, and surface tension of confined alkanes. J. Phys. Chem. C 113 (17), 7170–7180. https://doi.org/10.1021/jp8073915.

Song, C., Yang, D., 2017. Experimental and numerical evaluation of CO_2 huff-n-puff processes in Bakken Formation. Fuel 190 (15), 145–162. https://doi.org/10.1016/j.fuel.2016.11.041.

Song, Z., Song, Y., Guo, J., Zhang, Z., Hou, J., 2020. Adsorption induced critical shifts

of confined fluids in shale nanopores. Chem. Eng. J. 385, 123837. https://doi.org/10.1016/j.cej.2019.123837.
Teklu, T.W., Alharthy, N., Kazemi, H., Yin, X., Graves, R.M., AlSumaiti, A.M., 2014. Phase behavior and minimum miscibility pressure in nanopores. SPE Reservoir Eval. Eng. 17 (3), 396–403. https://doi.org/10.2118/168865-PA.
Tian, Y., Xiong, Y., Wang, L., Lei, Z., Zhang, Y., Yin, X., Wu, Y., 2019. A compositional model for gas injection IOR/EOR in tight oil reservoirs under coupled nanopore confinement and geomechanics effects. J. Nat. Gas Sci. Eng. 71, 102973. https://doi.org/10.1016/j.jngse.2019.102973.
Tuta, A.T., Singhal, A.K., 1998. Reservoir engineering aspects of oil recovery from low permeability reservoirs by air injection. In: SPE International Oil and Gas Conference and Exhibition. https://doi.org/10.2118/48841-MS.
Vishnyakov, A., Piotrovskaya, E., Brodskaya, E., Votyakov, E., Tovbin, Y., 2001. Critical properties of Lennard-Jones fluids in narrow slit-shaped pores. Langmuir 17 (14), 4451–4458. https://doi.org/10.1021/la001641a.
Wang, J., Liu, H., Qian, G., Peng, Y., 2021. Mechanisms and capacity of high-pressure soaking after hydraulic fracturing in tight/shale oil reservoirs. Petrol. Sci. 18, 546–564. https://doi.org/10.1007/s12182-020-00524-z.
Wang, L., Tian, Y., Yu, X., Wang, C., Yao, B., Wang, S., Philip, W., Wang, X., Yang, Z., Wang, Y., 2017a. Advances in improved/enhanced oil recovery technologies for tight and shale reservoirs. Fuel 210 (15), 425–445. https://doi.org/10.1016/j.fuel.2017.08.095.
Wang, Y., Zhang, Y., Liu, Y., Zhang, L., Ren, S., Lu, J., Wang, X., Fan, N., 2017b. The stability study of CO_2 foams at high pressure and high temperature. J. Petrol. Sci. Eng. 154, 234–243. https://doi.org/10.1016/j.petrol.2017.04.029.
Wei, J., Zhou, X., Zhou, J., Li, J., Wang, A., 2020. Recovery efficiency of tight oil reservoirs with different injection fluids: an experimental investigation of oil-water distribution feature. J. Petrol. Sci. Eng. 195, 107678. https://doi.org/10.1016/j.petrol.2020.107678.
Yang, G., Li, X., 2020. Modified Peng-Robinson equation of state for CO_2/hydrocarbon systems within nanopores. J. Nat. Gas Sci. Eng. 84 (12), 103700. https://doi.org/10.1016/j.jngse.2020.103700.
Yang, G., Fan, Z., Li, X., 2019. Determination of confined fluid phase behavior using extended Peng–Robinson equation of state. Chem. Eng. J. 378, 122032. https://doi.org/10.1016/j.cej.2019.122032.
Yao, J., Deng, X., Zhao, Y., Han, T., Chu, M., Pang, J., 2013. Characteristics of tight oil in triassic yanchang formation, Ordos Basin. Petrol. Explor. Dev. 40 (2), 161–169. https://doi.org/10.1016/S1876-3804(13)60019-1.
Yu, H., Lu, X., Fu, W., Wang, Y., Xu, H., Xie, Q., Qu, X., Lu, J., 2020. Determination of minimum near miscible pressure region during CO_2 and associated gas injection for tight oil reservoir in ordos basin, China. Fuel 263 (1), 116737. https://doi.org/10.1016/j.fuel.2019.116737.
Yu, H., Yang, Z., Luo, L., Liu, J., Cheng, S., Qu, X., Lei, Q., Lu, J., 2019. Application of cumulative-in-situ injection-production technology to supplement hydrocarbon recovery among fractured tight oil reservoirs: a case study in changqing oilfield, China. Fuel 242 (15), 804–818. https://doi.org/10.1016/j.fuel.2018.12.121.
Yu, Y., Li, L., Sheng, J., 2017. A comparative experimental study of gas injection in shale plugs by flooding and huff-n-puff processes. J. Nat. Gas Sci. Eng. 38, 195–202. https://doi.org/10.1016/j.jngse.2016.12.040.
Yu, Y., Meng, X., Sheng, J., 2016. Experimental and numerical evaluation of the potential of improving oil recovery from shale plugs by nitrogen gas flooding. Journal of Unconventional Oil and Gas Resources 15, 56–65. https://doi.org/10.1016/j.juogr.2016.05.003.
Zhang, J., Zhang, H., Ma, L., Liu, Y., Zhang, L., 2020. Performance evaluation and mechanism with different CO_2 flooding modes in tight oil reservoir with fractures. J. Petrol. Sci. Eng. 188, 106950. https://doi.org/10.1016/j.petrol.2020.106950.
Zhang, X., Xiao, P., Sun, C., Luo, G., Ju, Ju, Wang, X., Wang, H., Yang, H., 2018a. Optimal activated carbon for separation of CO_2 from (H_2 + CO_2) gas mixture. Petrol. Sci. 15, 625–633. https://doi.org/10.1007/s12182-018-0243-0.
Zhang, Y., Di, Y., Yu, W., Sepehrnoori, K., 2018b. A comprehensive model for investigation of carbon dioxide enhanced oil recovery with nanopore confinement in the bakken tight oil reservoir. SPE Reservoir Eval. Eng. 22 (1), 122–136. https://doi.org/10.2118/187211-PA.
Zheng, Z., Di, Y., Wu, Y., 2021. Nanopore confinement effect on the phase behavior of CO_2/hydrocarbons in tight oil reservoirs considering capillary pressure, fluid-wall interaction, and molecule adsorption. https://doi.org/10.1155/2021/2435930. Geofluids 2435930.
Zhou, X., Yuan, Q., Zhang, Y., Wang, H., Zeng, F., Zhang, L., 2019. Performance evaluation of CO_2 flooding process in tight oil reservoir via experimental and numerical simulation studies. Fuel 236, 730–746. https://doi.org/10.1016/j.fuel.2018.09.035.
Zhu, C., Guo, W., Wang, Y., Li, Y., 2021. Experimental study of enhanced oil recovery by CO_2 huff-n-puff in shales and tight sandstones with fractures. Petrol. Sci. 18, 852–869. https://doi.org/10.1007/s12182-020-00538-7.
Zou, C., Yang, Z., Hou, L., Cui, J., Wu, S., Lin, S., 2015. Geological characteristics and "sweet area" evaluation for tight oil. Petrol. Sci. 4, 606–617. https://doi.org/10.1007/S12182-015-0058-1.